Coupled Thermo-mechanical Micromechanics Modeling of the Influence of Thermally Grown Oxide Layer in an Environmental Barrier Coating System

Trenton M. Ricks[1*]
Steven M. Arnold[1]
and
Bryan J. Harder[2]

[1]Multiscale and Multiphysics Modeling Branch, NASA Glenn Research Center, Cleveland, OH 44135

[2]Environmental Effects and Coatings Branch, NASA Glenn Research Center, Cleveland, OH 44135

Keywords: *environmental barrier coating, thermally grown oxide, micromechanics*

ABSTRACT

Environmental Barrier Coatings (EBCs) have emerged as a promising means of protecting silicon based ceramic matrix composite (CMC) components for high temperature applications (*e.g.*, aircraft engines). EBCs are often used to protect an underlying material (substrate) such as silicon carbide from extreme thermal/chemical environments. In a typical CMC/EBC system, an EBC may or may not be adhered to an underlying substrate with a bond coat (*e.g.*, silicon). Irrespective, systems that utilize EBCs are susceptible to a number of failure modes including oxidation/delamination, recession, chemical attack and dissolution, thermomechanical degradation, erosion, and foreign object damage. Current work at NASA Glenn Research Center is aimed at addressing these failure modes in EBC systems and developing robust analysis tools to aid in the design process. The Higher-Order Theory for Functionally Graded Materials (HOTFGM), a precursor to the High-Fidelity Generalized Method of Cells micromechanics approach, was developed to investigate the coupled thermo-mechanical behavior of functionally graded composites and will be used herein to assess the development and growth of a low-stiffness thermally grown oxide (TGO) layer in EBC/CMC systems without a silicon bond coat. To accomplish this a sensitivity study is conducted to examine the influence of uniformly and nonuniformly grown oxide layer on the associated driving forces leading to mechanical failure (spallation) of EBC layer when subjected to isothermal loading.

Trenton M. Ricks, Multiscale and Multiphysics Modeling Branch, NASA Glenn Research Center, Cleveland, OH 44135.
Steven M. Arnold, Multiscale and Multiphysics Modeling Branch, NASA Glenn Research Center, Cleveland, OH 44135.
Bryan J. Harder, Environmental Effects and Coatings Branch, NASA Glenn Research Center, Cleveland, OH 44135.

INTRODUCTION

Over the past decade significant progress has been made with respect to understanding, manufacturing and deploying silicon-based ceramic matrix composites (CMCs) such as silicon carbide (SiC)/SiC for use within turbine engines. The use of such low density, high temperature capable materials, enables the design and operation of more fuel efficient engines, which demand less cooling, and consequently reduce greenhouse gas emissions such as CO_2 and NO_x. However, at high temperatures these materials rapidly oxidize and form a volatile hydroxide species in the presence of water vapor, which is prevalent in combustion environments [1-5]. In order to limit this oxidation and stop the recession of these CMCs, environmental barrier coatings (EBCs) have been developed and deployed as a requirement for use of Si-based CMCs in turbine engine environments [6-7]. Current state of the art EBC systems consist of a rare earth silicate topcoat such as $Yb_2Si_2O_7$ with a silicon (Si) bond coat [8]. The disilicate top coat limits the recession, but oxidation can still occur at the interface between the bond coat and the topcoat (EBC) or at the substrate in the case of a fully oxidized or absent silicon bond coat. This oxidation process results in the development of a thermally grown oxide (TGO). Observations have indicated that once this TGO reaches a critical thickness, transverse cracking and/or delamination at the TGO/EBC or TGO/CMC interface can cause spallation and failure of the EBC, which exposes the substrate and can cause premature failure in a CMC component. Slowing TGO formation and understanding failure criteria in EBC coated CMCs is critical to the lifetime of these Si-based components.

In this paper, two EBC/CMC systems, *i.e.*, a two layer (EBC/CMC) and three layer (EBC/TGO/CMC) system, will be analyzed using NASA's HOTFGM micromechanics analysis code in an attempt to identify and assess how the resulting in-situ mechanical driving forces develop and evolve as the TGO thickness and/or location(s) evolve.

HIGHER ORDER THEORY FOR FUNCTIONALLY GRADED (HOTFGM) MATERIALS

The Higher-Order Theory for Functionally Graded Materials (HOTFGM), a precursor to the High-Fidelity Generalized Method of Cells micromechanics approach [9], was developed to investigate the coupled thermo-mechanical behavior of functionally graded materials [9]. Figure 1 describes the general capabilities of the HOTFGM code. In the mid to late 1990's, HOTFGM 2-D was employed [11-14] to investigate the effect of material and geometric parameters on the interlaminar stresses (including free edge effects) of a three layer (*i.e.*, top coat (thermal barrier coating)/bond coat/substrate) sandwich plate configuration subjected to a thermal load. Analyses included the examination of monolithic layers with both smooth and rough bond coat/top coat interfaces as well as the effect of inelastic (*i.e.*, creep) material behavior [14]. Note the influence of interfacial roughness played a key role in the initiation and propagation of delamination.

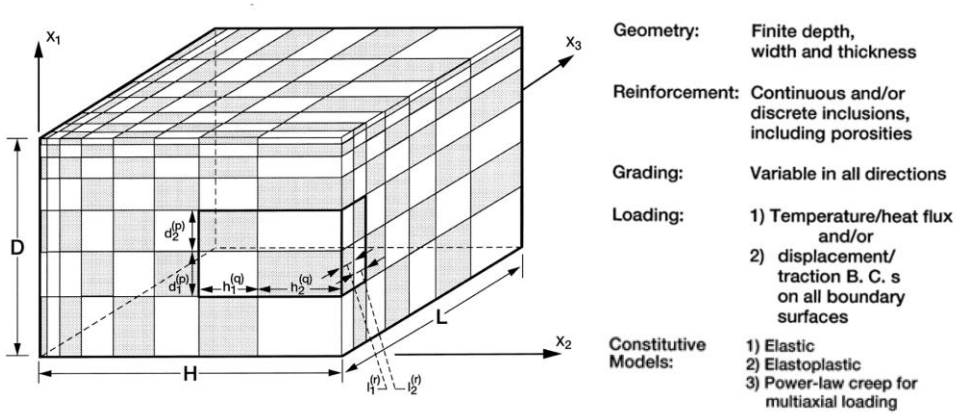

Figure 1. Schematic of functionally graded material (HOTFGM-3D) wherein gradients in both loading and microstructure are allowed in all three directions.

HOTFGM-2D represents a geometric model of a heterogeneous composite having finite dimensions in the x_2–x_3 plane and extending to infinity in the x_1 direction. In the x_2–x_3 plane, the material can be functionally graded with an arbitrary distribution of inclusions of arbitrary cross section. The loading applied to the "plate" may involve an arbitrary temperature or heat flux distribution and mechanical effects represented by a combination of surface displacements and/or tractions in the x_2–x_3 plane, and a uniform stress in the x_1 direction (in this paper that average stress is taken to be zero, *i.e.*, plane stress condition). The functionally graded microstructure in the x_2–x_3 plane is modeled by discretizing the heterogeneous composite (plate's) cross section into N_q and N_r generic cells in the intervals $0 \leq x_2 \leq H$, $0 \leq x_3 \leq L$. The generic cell (q, r) used to construct the composite, highlighted in Figure 1, consists of four subcells designated by the pair (β γ), where each index β , γ takes on the values 1 or 2 which indicate the relative position of the given subcell along the x_2 and x_3 axis, respectively. The indices q and r, whose ranges are q = 1, 2,…, N_q and r = 1, 2,…, N_r , identify the generic cell in the x_2 –x_3 plane. The dimensions of the generic cell along the x_2 and x_3 axes, $h_1^{(q)}$, $h_2^{(q)}$, and $l_1^{(r)}$, $l_2^{(r)}$, can vary in an arbitrary fashion such that

$$H = \sum_{q=1}^{N_q} \left(h_1^{(q)} + h_2^{(q)}\right) \; ; \qquad L = \sum_{r=1}^{N_r} \left(l_1^{(q)} + l_2^{(q)}\right) \tag{1}$$

Given the applied thermomechanical loading, an approximate solution for the temperature and displacement fields is constructed based on volumetric averaging of the field equations together with the imposition of boundary and continuity conditions in an average sense between the sub-volumes used to characterize the material's microstructure. A higher-order representation of the temperature and displacement fields is necessary in order to capture the local effects created by the thermomechanical field gradients, the microstructure of the composite, and the finite dimensions in the functionally graded directions, see [9] for more details regarding the mathematical formulation.

A schematic of the specific three layer laminated plate investigated is shown in Figure 2. Wherein the overall width of the specimen (L = 10 mm) and thickness (H = 3.175 mm); the width was chosen to ensure uniform fields away from the free

edge. The total number of cells in the x_2 direction is N_q = 85, while that in the x_3 direction is N_r = 166. This results in 170 subcells being used in the x_2 direction (*i.e.*, EBC = 35, TGO = 4, and substrate = 131) while that in the x_3 direction is 332. A mesh sensitivity study was conducted to ensure that results away from the free edge had converged and subcell aspect ratio had minimal effect on stress results. As indicated in Figure 2, the primary loading is that due to isothermal cooling linearly from the stress free reference temperature of T = 1482 C (2700 ºF) to 38.7 C (102 ºF). Constituent deformation behavior is assumed to follow Hooke's law. The thermoelastic properties of all three constituent materials ($Yb_2Si_2O_7$ - EBC, SiO_2 TGO, and Hexoloy SiC substrate) are all assumed to be isotropic and are given in Table I. Finally, in all simulations the total system thickness, H, was held fixed; thus as TGO thickness increases substrate thickness commensurately decreases (or is "consumed") as observed experimentally.

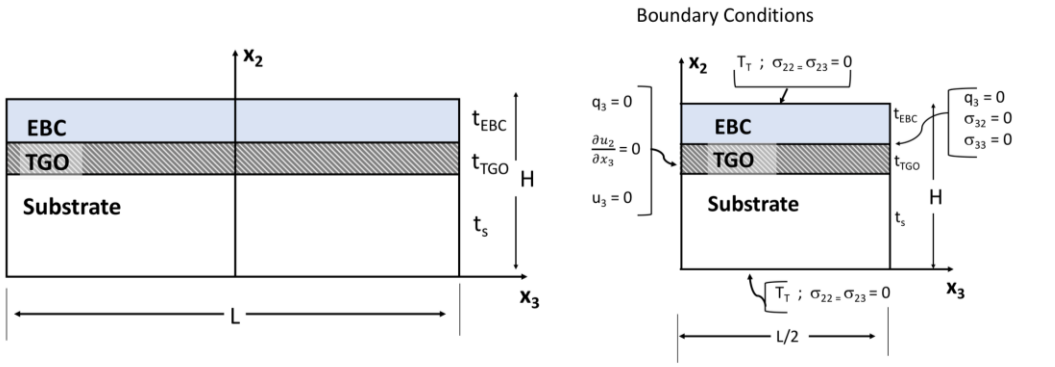

Figure 2. Schematic showing the three layer system, with geometry and applied thermal and mechanical boundary conditions.

Table I. CONSTITUENT ISOTROPIC THERMOELASTIC PROPERTIES

Material	Thickness (mm)	Modulus (GPa)	Poisson Ratio	CTE ($x10^{-6}$ K^{-1})	Conductivity (W/m-K)
$Yb_2Si_2O_7$ (EBC)	0.175	200	0.27	4.5	1.25
SiO_2 (TGO)	0.001 0.002 0.004 0.008 0.016	35	0.17	10	1.4
Hexoloy SiC (Substrate)	3*	400	0.17	5.25	30

* Initial thickness assuming no TGO

RESULTS

Uniform layers

A variety of simulations were performed to assess the influence of TGO growth, *i.e.*, thickness increase of a continuous uniform TGO layer, on the stress state of a three layer EBC/TGO/CMC system after thermal cooldown. A two layer baseline case, of EBC and CMC substrate is shown in Figure 3; wherein Figure 3a-b show a contour plot of the mean (I_1) and effective stress ($\sqrt{3J_2}$), respectively. This baseline represents an idealized "pristine" condition of an EBC/CMC system. Stress analysis results reveal that while some stress concentrations are observed near the free edge ($x_3/L = 0.5$) at the EBC/substrate interface, the far-field stresses are relatively uniform away from the free edge. The CTEs of the EBC and substrate are similar, and the modulus of the EBC is half of the substrate. As a result of the CTE mismatch between EBC and substrate (see Table I), the more compliant EBC layer develops a compressive stress state, as shown in Figure 3a. In contrast, when a three layer system is simulated (one in which a thermally grow oxide (with a substantially larger CTE) layer of 16 μm exists), the stress states in the EBC and substrate are shown to be virtually identical to the baseline case, except now a significant tensile triaxial stress state emerges in the TGO layer (see contour plots in Figure 4a-b). Furthermore, both mean and effective stress states in the TGO were determined to be uniform away from the free edge and throughout the TGO thickness. Figure 5 shows stress component (*i.e.*, σ_{11}, σ_{22}, σ_{33}, and σ_{23}), mean stress, and effective stress profiles as a function of through thickness location along the symmetry plane. Interestingly, the TGO thickness has no significant (< 1%) effect on the resulting stress state in the system as only minor differences were observed as the TGO layer thickness was increased. Additionally, the σ_{11} and σ_{33} stress profiles were found to be similar except for a slight variation through the thickness of the substrate layer. However, as shown in Figure 5b and Figure 5d, respectively, σ_{22} and σ_{23} were negligible indicating the absence of any peel and/or shear driving forces that could lead to EBC spallation. A plot of the σ_{11} stress profile near the substrate/TGO and TGO/EBC interfaces is shown in Figure 6 for a 0, 1, 2, 4, 8, and 16 μm thick uniform TGO. While the location of the stress discontinuity changed depending on TGO thickness (as expected), the magnitude of the tensile stress within the TGO is nearly identical for all thicknesses.

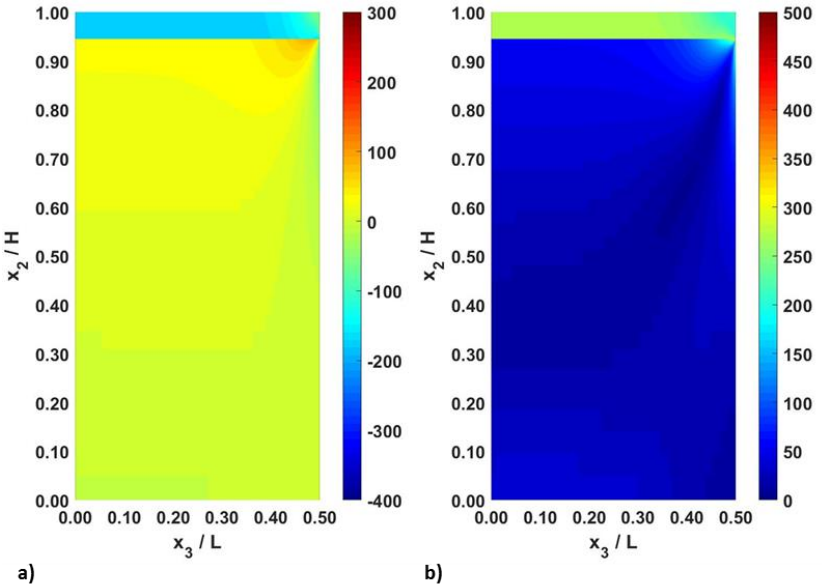

Figure 3. a) Mean and b) effective stress distributions (units of MPa) for a two layer system (EBC and substrate only).

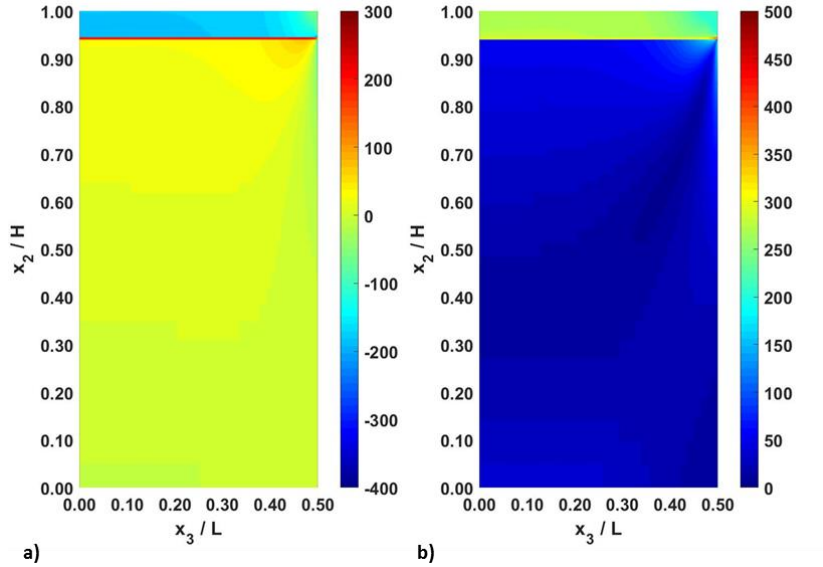

Figure 4. a) Mean and b) effective stress distributions (units of MPa)for a three layer system with a 16 μm thick TGO.

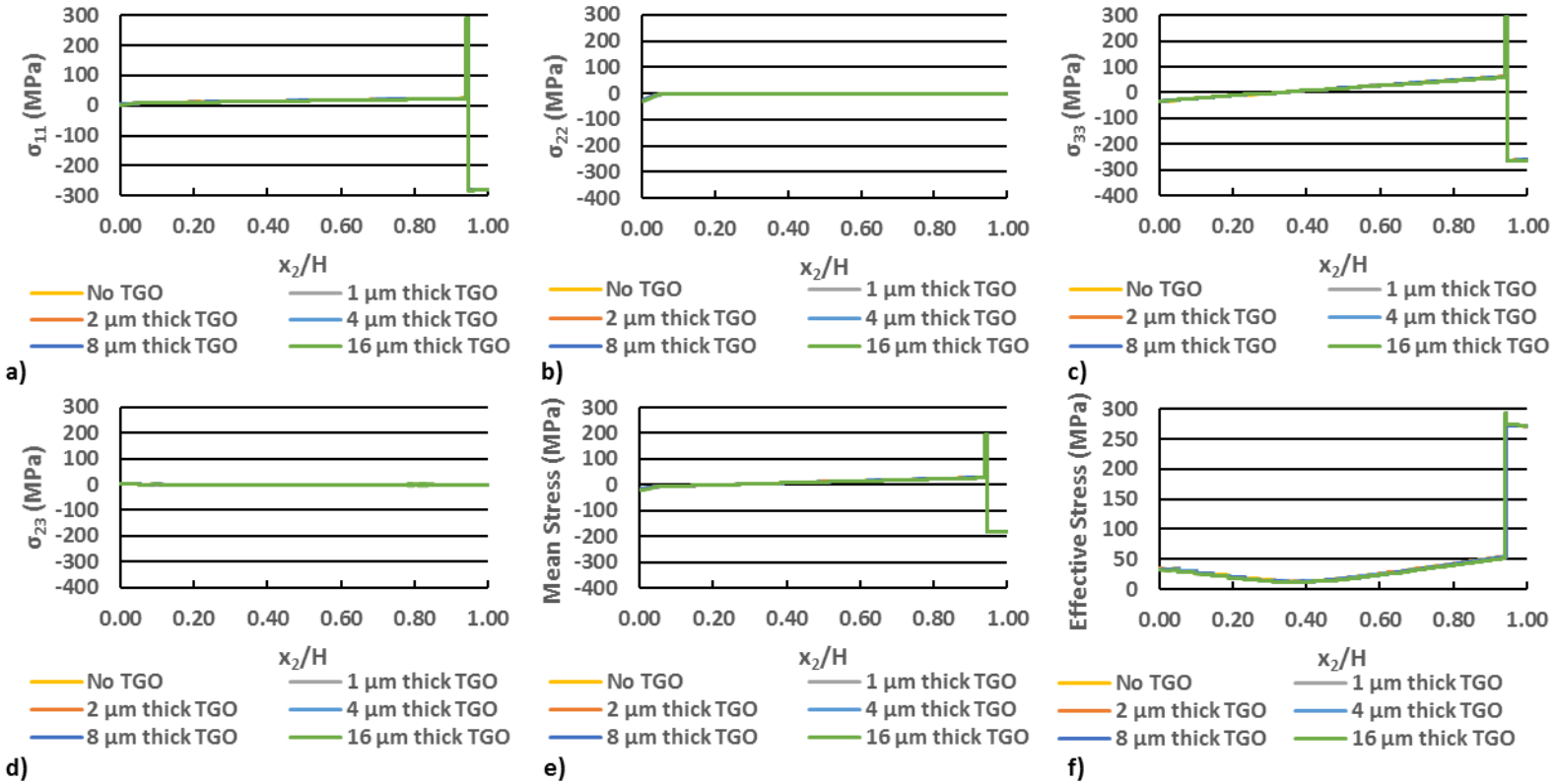

Figure 5. Stress distributions for a three layer system with a uniform but varying TGO thickness (*i.e.*, 1, 2, 4, 8, 16 µm) compared against a two layer system without a TGO.

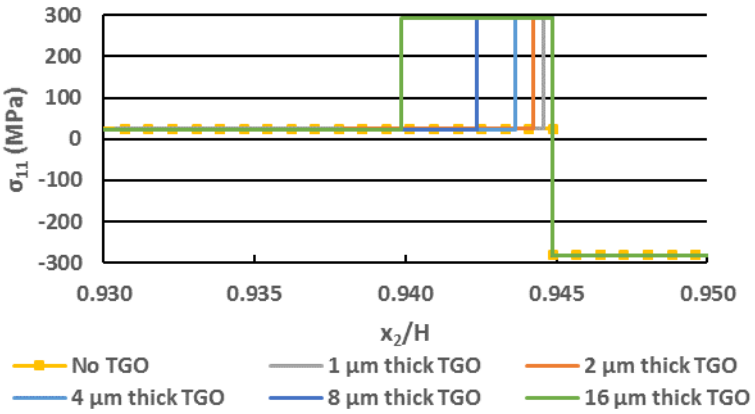

Figure 6. Out-of-plane normal stress (σ_{11}) along the symmetry plane ($x_3 = 0$) near the substrate/TGO and TGO/EBC interfaces for a three layer system and the substrate/EBC interface for the two layer system.

Discontinuous TGO Layers

Given that the above continuously uniform layered system results exhibited no change in mechanical driving forces as a function of TGO growth, no critical TGO thickness, that would induce failure, could be established. This is contrary to experimental observation which consistently showed lower TGO life times as a function of increased TGO thickness. Consequently, drawing upon prior thermal barrier coating work [11, 14] with respect to interfacial roughness between top coat and bond coat and current EBC/CMC microscopy observations, it was decided to investigate geometric nonuniformites in the TGO growth pattern. To this end, discontinuous TGO "islands" were inserted between the substrate and EBC interface, as a first approximation (albeit severe) to capture nonuniform TGO growth effects. The objective of this analysis is to *qualitatively*, not *quantitatively* identify the potential driving forces that could cause failure.

Both thin (1 µm) and thick (16 µm) TGO layers were simulated with an island width W_{TGO} = ~301 µm. As before the TGO was assumed to grow into the substrate and thus decrease the substrate thickness. As a result, these TGO island layers were separated by substrate material (~60 µm width, W_{SUB}). The effect of TGO island width and spacing will be considered in a future work. A schematic of this geometrical arrangement (with EBC (blue layer), TGO (red rectangles) and CMC substrate (green)) involving only the first ~550 µm out of 5000 µm ($L/2$) in the x_3 direction is shown in Figure 7 along with two locations where stresses will later be plotted. Since symmetry boundary conditions were modeled, the initial TGO island width was set to half its full width.

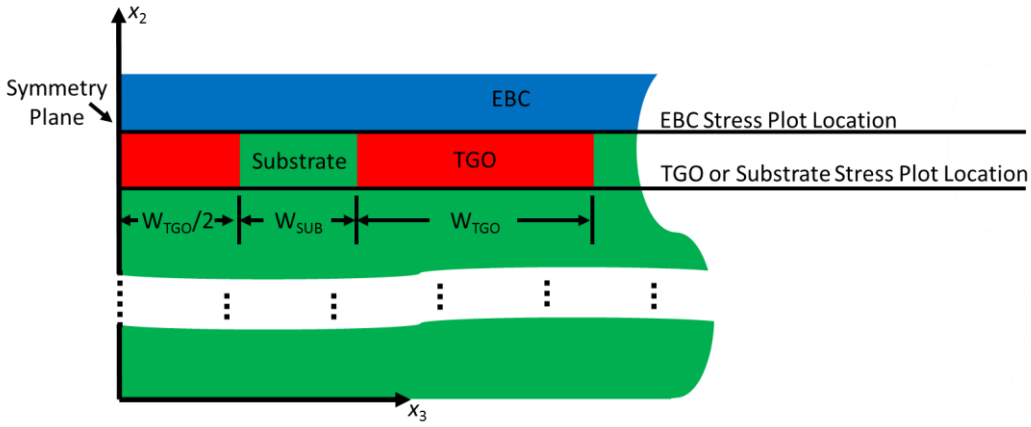

Figure 7. Schematic showing discontinuous TGO layer geometry.

Figure 8 depicts contour plots of the mean and effective stresses for a three layer EBC/TGO/CMC system with discontinuous thin (1 μm) TGO islands. In general, the stress state is similar to the uniform TGO results, as one might expect. However, slight stress concentrations can be observed in between the TGO islands. As the thickness of the TGO was increased (by a factor of 16), the magnitude of these stresses increased dramatically as shown in Figure 9.

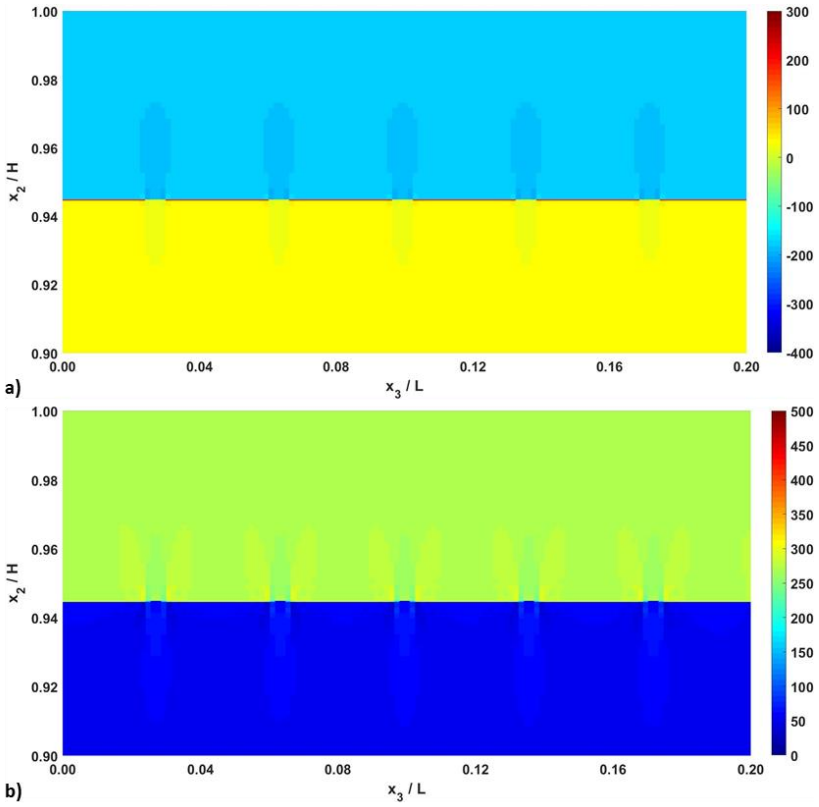

Figure 8. a) Mean and b) effective stress distributions (units of MPa) for a three layer system with discontinuous thin TGO layers.

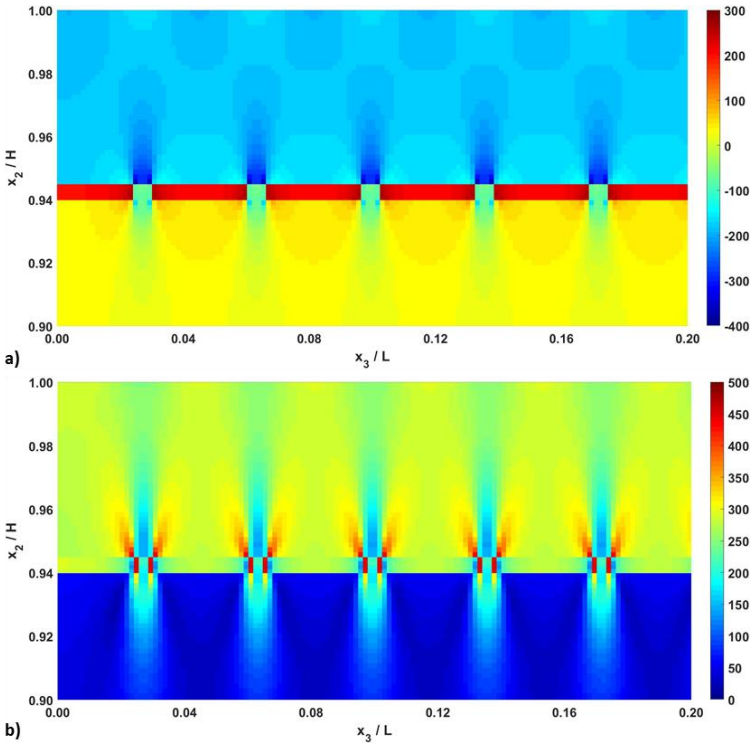

Figure 9. a) Mean and b) effective stress distributions (units of MPa) for a three layer system with discontinuous thick TGO layers.

Figure 10a-b contain the mean and effective stress, respectively in the EBC (taken along the EBC/TGO interface, see Figure 7), and TGO and substrate (along the TGO/substrate interface, see Figure 7) for the thin TGO system. For this system, the TGO and substrate are predominately in tension while the EBC is in compression. Note that although the mean and effective stresses for the TGO and substrate are plotted at the same vertical position, discontinuities in the stresses occur at the TGO/substrate interfaces. The effective stress (Figure 10b) in all layers is similar with the exception of the TGO/substrate transition regions.

Figure 10c-d contain similar plots but now for the thick discontinuous TGO system. Slight differences in the interior TGO stress state were observed but a marked increase at the edges of TGO islands appeared. The substrate, however, transitions from a mild triaxial state of tension to that of compression. And although the EBC remains in compression, a significantly higher compressive triaxial stress state was observed near TGO/substrate interfaces. Both the EBC and substrate had higher effective stresses at these interfaces for the thick TGO system while the effective stress decreased significantly as the edges of the TGO islands were approached.

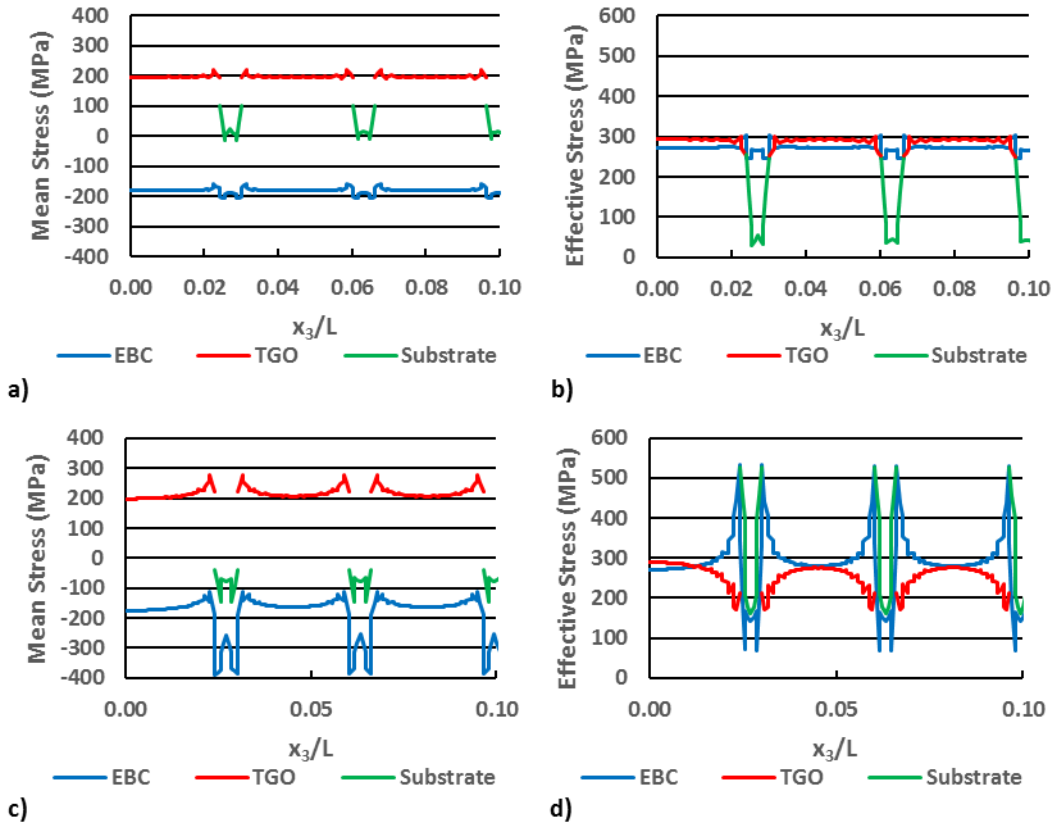

Figure 10. a) Mean and b) effective stress distributions in the EBC and at the TGO/substrate interface for a three layer system with 1 μm thick by 301 μm discontinuous TGO layers. Similar c) mean and d) effective stress distributions for 16 μm thick by 301 μm discontinuous TGO layers.

To better visualize the influence of TGO thickness effect, Figure 11a-c show the individual stress components in the EBC for both the thin and thick TGO systems. Note that a plot of σ_{33} was not included as it is similar to the σ_{11} component. The σ_{11} stress component was observed to be compressive and shown to be independent of TGO thickness when away from the TGO/substrate interface regions where a significant increase in compressive state is observed for thick TGO islands. A slight increase in σ_{11} was observed near the center of a TGO island. A tensile peel stress (σ_{22}) state, however, significantly increased as the TGO thickness increased suggesting a potential for EBC spallation in the vicinity of a TGO island. Significantly higher shear stresses were also predicted to occur near these interface regions as well. While the mean stress in the EBC was compressive (Figure 10a,c), significant *tensile* peel stresses occurred near the interface regions and became more pronounced as the TGO thickness increased.

Figure 11d-f contain the individual TGO and substrate stress components for the thin and thick TGO systems. Clearly, the σ_{11} TGO stress state is tensile yet independent of TGO thickness, while a transition from slight tension to slight compression occurred in the substrate as the TGO layer increased to 16 μm. Additionally, significant shear stresses developed at the TGO/substrate interfaces. However, the peel, σ_{22}, stress in the substrate became significantly more compressive while the slight tensile TGO peel stress increased dramatically with TGO thickness. Hence, as the TGO thickness

increases, both the peel and shear stresses increase in the EBC and TGO at the geometric discontinuities.

Recall that for a uniform TGO thickness, the peel and shear stresses in all layers were negligible. Based on these results, it is hypothesized that these significant peel and shear stresses at material discontinuities can lead to EBC spallation (failure) and thus could be used to establish a critical TGO thickness that one needs to stay below to ensure a robust coating. The peel stresses would cause both the EBC to pull away from the TGO and the TGO to pull away from the underlying substrate. When coupled with the high shear stresses in the EBC and TGO, any cracks that had developed in the TGO due to the high σ_{11} and σ_{33} stresses would likely be driven across the TGO or through the EBC resulting in EBC spallation.

CONCLUSIONS

In this study, coupled elastic thermo-mechanical simulations of a silicon based ceramic matrix composite (CMC) were performed using the Higher-Order Theory for Functionally Graded Materials (HOTFGM) micromechanics approach. An environmental barrier coating (EBC), utilized to protect the underlying silicon substrate, was included in the analysis. The influence of a low-stiffness thermally grown oxide (TGO) layer of multiple thicknesses was investigated. Both uniform and discontinuous TGO layers were considered. For uniform TGO layers, the TGO thickness had a negligible effect on the stress state of the system. When discontinuous TGO layers were considered however, significant peel and shear stresses were predicted to occur in both the TGO and EBC near these discontinuities. These stresses could explain the onset and evolution of TGO damage and ultimately EBC spallation when a critical TGO thickness is reached. The idealized geometry considered in this study represents a first step at understanding the influence of TGO geometric nonuniformity on the stress state in a CMC/EBC system. Ongoing work is addressing the influences of TGO undulation in the presence of a bond coat, and thermal gradients on the life of EBC/CMC systems in steam environments.

ACKNOWLEDGMENT

This work was supported through NASA's Transformational Tools and Technologies (TTT) program.

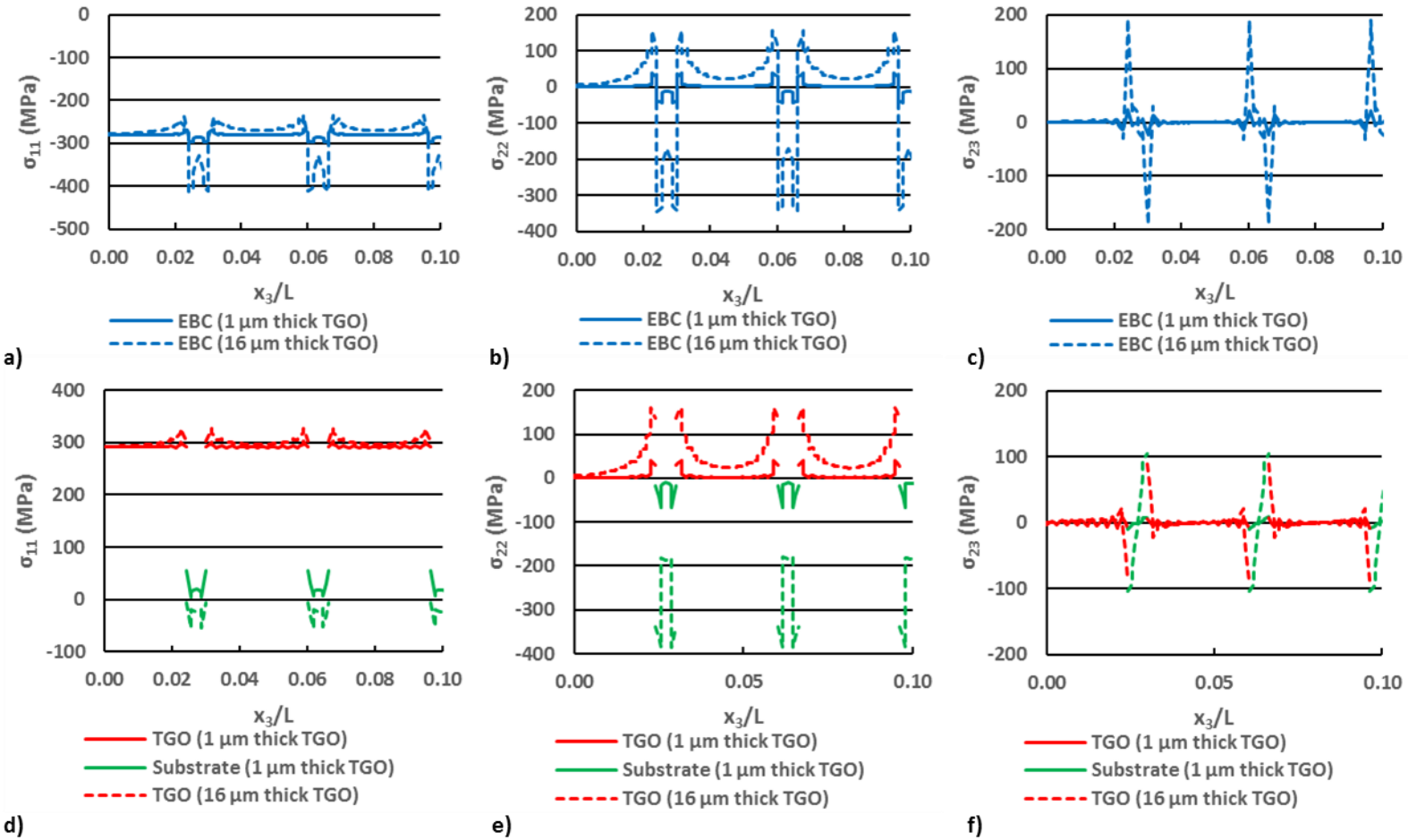

Figure 11. a) Out-of-plane (σ_{11}) and b) in-plane (σ_{22}) normal stresses and c) the shear stress (σ_{23}) in the EBC. d) σ_{11}, e) σ_{22}, and f) σ_{23} at the TGO/substrate interface. Stress/strain curves are plotted across the width for discontinuous 1 µm and 16 µm thick by 301 µm TGO layers.

REFERENCES

1. Deal, B.E. and A.S. Grove. 1965. “General Relationship for the Thermal Oxidation of Silicon, *J. Appl. Phys.*, 36(12):3770–3778.
2. Jacobson, N.S. 1993. “Corrosion of Silicon-Based Ceramics in Combustion Environments,” *J. Am. Ceram. Soc.*, 76(1):3–28.
3. Opila, E.J. 1994. “Oxidation Kinetics of Chemically Vapor-Deposited Silicon Carbide in Wet Oxygen,” *J. Am. Ceram. Soc.*, 77(3):730–736.
4. Smialek, J.L., R.C. Robinson, E.J. Opila, D.S. Fox, and N.S. Jacobson 1999. “SiC and Si3N4 Recession due to SiO2 Scale Volatility under Combustor Conditions,” *Adv. Compos. Mater.*, 8(1):33–45.
5. Opila, E.J., J.L. Smialek, R.C. Robinson, D.S. Fox, and N.S. Jacobson. 1999. “SiC Recession Caused by SiO2 Scale Volatility under Combustion Conditions : II , Thermodynamics and Gaseous-Diffusion Model,” *J. Am. Ceram. Soc.*, 82(7):1826–1834.
6. Lee, K.N. 2000. “Current Status of Environmental Barrier Coatings for Si-Based Ceramics,” *Surf. Coat. Technol.*, 133–134: 1–7.
7. Lee, K.N., D.S. Fox, J.I. Eldridge, D. Zhu, R.C. Robinson, N.P. Bansal, and R.A. Miller. 2003. “Upper Temperature Limit of Environmental Barrier Coatings Based on Mullite and BSAS,” *J. Am. Ceram. Soc.*, 86(8):1299–1306.
8. Lee, K.N., D.S. Fox, and N.P. Bansal. 2005. “Rare Earth Silicate Environmental Barrier Coatings for SiC/SiC Composites and Si3N4 Ceramics,” *J. Eur. Ceram. Soc.*, 25:1705–1715.
9. Aboudi, J., S.M. Arnold, and B.A. Bednarcyk. 2013. *Micromechanics of Composite Materials: A Generalized Multiscale Analysis Approach*, Elsevier, Oxford, UK.
10. Aboudi, J., M-J. Pindera, and S.M. Arnold. 1999, ‘‘Higher-Order Theory For Functionally Graded Materials”, *Compos. B*, 30:777-832.
11. Arnold, S. M., Aboudi, J., Pindera, M-J. 1995. ‘‘Thermally-Induced Interlaminar Stresses in TBC-Protected Plate: A Material and Geometric Parametric Study,” HITEMP Review 1995, Vol. II, CP 10178, pp. 34:1-14.
12. Pindera, M-J., J. Aboudi, and S.M. Arnold, 1997. ‘‘Microstructural Effects in Functionally Graded Thermal Barrier Coatings,” in *Functionally Graded Materials*, I. Shiota and Y. Miyamoto, eds. Netherlands: Elsevier Science B.V., pp. 113-121.
13. Pindera, M-J., J. Aboudi, and S.M. Arnold. 1998. ‘‘The Effect of Microstructure on the Response of Functionally Graded Thermal Barrier Coatings”, *J. Am. Ceram. Soc.*, 81(6):1525-1536.
14. Pindera, M-J., J. Aboudi, and S.M. Arnold. 2000. “The Effect of Interface Roughness and Oxide Film Thickness on the Inelastic Response of Thermal Barrier Coatings to Thermal Cycling”, *J. Mat. Sci. Engrg. A*, 284:158-175.